Eur. Phys. J. Plus (2025) 140:616
https://doi.org/10.1140/epjp/s13360-025-06531-6

THE EUROPEAN PHYSICAL JOURNAL PLUS

Regular Article

Impact of higher twist effects on determining the polarized parton distribution functions using Gegenbauer polynomials

Hamed Abdolmaleki[1,2,a], **Abolfazl Mirjalili**[3,b], **Reyhaneh Farashaeian**[3,c], **S. Mohammad Moosavi Nejad**[3,d], **Javad Sheibani**[4,e], **Shahin Atashbar Tehrani**[4,5,f]

[1] Department of Physics, Faculty of Science, Malayer University, Malayer, Iran
[2] School of Physics, Institute for Research in Fundamental Sciences (IPM), Tehran, Iran
[3] Department of Physics, Yazd University, P.O. Box 89195-741, Yazd, Iran
[4] School of Particles and Accelerators, Institute for Research in Fundamental Sciences (IPM), P.O. Box 19395-5531, Tehran, Iran
[5] Department of Physics, Faculty of Nano and Bio Science and Technology, Persian Gulf University, 75169 Bushehr, Iran

Received: 26 February 2025 / Accepted: 6 June 2025

Abstract Parton Distribution Functions (PDFs) are important quantities that describe the distributions of momentum and spin of partons inside a nucleon. Their exact determination is crucial for precision tests of the Standard Model and also for making predictions of experimental results in high energy colliders. Gegenbauer polynomials are a set of orthogonal polynomials which could be used to parameterize PDFs. These polynomials are solutions to a second-order differential equation and depend on the two parameters: the degree of polynomials and a constant known as the Gegenbauer coefficient. By fitting the experimental data with a combination of Gegenbauer polynomials, one can extract the values of unknown parameters including these coefficients, which in turn can provide a physical insight into the structure of proton. The use of Gegenbauer polynomials in PDFs has several advantages over other parameterizations; they have better convergence properties and can more accurately capture the shape of the PDFs at high momentum fractions. Through this work we use these polynomials to parameterize the polarized PDFs (PPDFs) where the positivity constraint enforced on them. In continuation from two analysis with and without considering the higher twist effects we determine the polarized structure functions of proton, neutron and deuteron at NLO accuracy. Considering all available data, specifically including final JLAB **CLAS/EG1b** data for proton and deuteron, we show that taking the higher twist effect is necessary to determination of the PPDFs. Investigation of the polarized Bjorken sum rule and proton helicity sum rule is also conducted to verify the fitting results. The findings show expected alignment with the existing data and certain parametrization models.

1 Introduction

Quantum Chromodynamics (QCD) is a well-constructed theory describing the strong interactions between partons in a way that is consistence with the experimental findings. The QCD includes the necessary tools for the scale evolution of nucleon structure functions. Based on this, parton distribution functions (PDFs) at initial energy scale, which are referred to as the non-perturbative part of evolution process, can be used to characterize nucleons in perturbative QCD (pQCD) framework. The fragmentation functions (FFs) and PDFs together constitute the non-perturbative components of hadron production and lepton-hadron scattering processes, respectively, which are necessary for determining physical quantities including branching ratios, decay rates, and cross sections [1, 2]. The PDFs and FFs are typically related to partons. PDFs refer to the probabilities of finding partons carrying a specific fraction of the spin and momentum of a nucleon, while FFs describe the probability densities for a specific parton to fragment into an expected hadron, carrying away a fraction of its momentum. Among all measurable quantities, polarized structure functions are experimental observable which provide important information about the distribution of momenta as well as the spin of partons inside the nucleon. Accurate determination of these functions is crucial for our understanding about the origin of the nucleon spin and for testing theoretical models describing nucleon structure. The polarized parton distribution function (PPDF) determination with their estimated uncertainties has been presented in diverse studies [3–19]. The key differences between the various studies stem from

[a] e-mail: Abdolmaleki@ipm.ir (corresponding author)
[b] e-mail: A.Mirjalili@yazd.ac.ir
[c] e-mail: r.farashaeian@stu.yazd.ac.ir
[d] e-mail: mmoosavi@yazd.ac.ir
[e] e-mail: j.sheibani@ipm.ir
[f] e-mail: Atashbar@ipm.ir

Published online: 01 July 2025

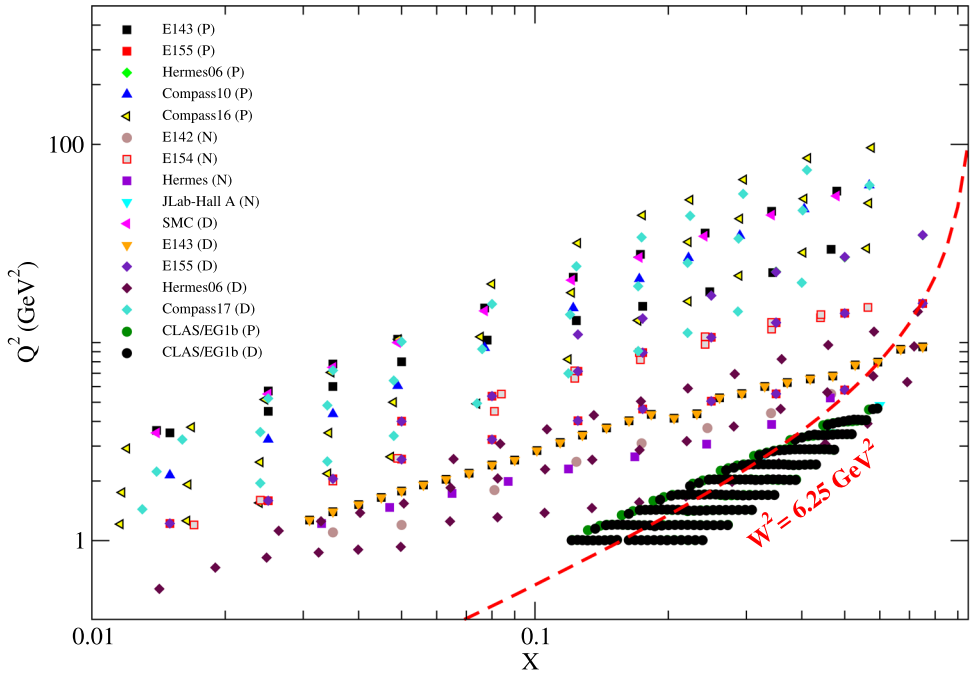

Fig. 1 Different experiments of polarized structure functions, xg_1^N, data for proton, deuteron and neutron in the x and Q^2 plane. The dashed line represents the kinematic W^2 cut on the data ($W^2 \geq 6.25$ GeV^2) which is used to avoid the presence of dynamical higher twists effect

the specific choices made regarding the used experimental data, the parameterization, their estimated uncertainties, and the QCD corrections applied during the analysis process such as heavy quark treatment and higher-twist correction.

To determine the polarized and unpolarized distribution functions many different approaches have extensively been used. The predominant approach in selecting the parametrization form, in addition to the more standard approches, involves the use of orthogonal Bernstein and Jacobi polynomials, which have implications for extracting the polarized parton distribution functions of gluons and sea quarks. These parametrization forms have lack of convergence which leads to a reduction in the number of free parameters. For further information, please refer to references [20–22]. Among them, Gegenbauer polynomials have also been applied to parameterize polarized parton distribution functions similarly to the unpolarized case so that the polarized Gegenbauer coefficients can be extracted from experimental data. They provide a comprehensive insight over the polarized quark and gluon distributions inside the nucleon. Using the Gegenbauer polynomials in determining the polarized structure functions has several advantages [23]. In fact, the orthogonality of Gegenbauer polynomials allows for a systematic expansion of the polarized structure functions in terms of the polarized Gegenbauer coefficients [24, 25]. Furthermore, the Gegenbauer polynomials provide a better convergence at high momentum fractions in comparing with other parametrization models, such as the commonly used series expansion in terms of Legendre polynomials [26].

Gegenbauer polynomials are orthogonal with respect to the weight function $x^\alpha(1-x)^\beta$, which reflects the typical shape of polarized PDFs. This orthogonality leads to faster convergence when approximating analytic functions, allowing significant error reduction near the high momentum fraction region $x \to 1$ even with a limited number of terms (e.g., three). In contrast, ordinary polynomials like $a + bx + cx^2$ lack orthogonality and generally require more terms to achieve similar accuracy. Thus, Gegenbauer polynomials, being naturally adapted to the polarized PDF shape through their weighted orthogonality, optimize the approximation error. These considerable advantages motivate us to use the Gegenbauer polynomials in extracting the polarized structure functions which provides a powerful tool for understanding the spin distributions inside the nucleon as well as testing theoretical models describing the nucleon structure. In addition to these aspects, two important ingredients of our QCD analysis include: Initially, the representation of polarized parton densities using Gegenbauer polynomials is designed to meet the positivity requirement. Secondly, we employ the higher twist (HT) effect in our analysis to enhance the outcomes. Two approaches, **Fit A** and **FitB**, are being considered to show the upcoming progress, with **Fit A** not involving the HT effect and **Fit B** involving it.

The paper is structured in the following way. The QCD framework is presented in Sec.2. Fitting content which is employed in our QCD analysis, is discussed in Sec.3. Next section, Sec.4 focuses on explaining the datasets and the minimization technique. Discussion on the parametrization of polarized parton densities in global analysis is presented in Sec.5, along with topics such as the inverse Mellin technique. The findings from Bjorken sum rule and proton helicity sum rule, utilizing Gegenbauer parametrization in **Fit B** approach, are discussed in Sec.6. Ultimately, we present our conclusion in Sec.7.

2 QCD framework for inclusive and semi-inclusive polarized DIS

Basically, our understanding of QCD as well as the nucleon structure profoundly depends on the deep inelastic scattering (DIS) processes. One of the features of polarized DIS is the fact that more than half of the present data are at moderate Q^2 and W^2 ($Q^2 \sim 1-5\,GeV^2,\ 4\ GeV^2 < W^2 < 10\ GeV^2$), or in the so-called *preasymptotic* region. This is, especially, the case for the very precise experiments performed at the Jefferson Laboratory. So, in contrast to the unpolarized case this region cannot be excluded from the analysis. As was shown in Ref. [27], to confront correctly the QCD predictions to the experimental data including the preasymptotic region, the *nonperturbative* higher twist (powers in $1/Q^2$) corrections to the nucleon spin structure functions have to be taken into account too.

In QCD, the spin structure function g_1 has the following form for $Q^2 >> \Lambda^2$ (the nucleon target label N is not shown):

$$g_1(x,Q^2) = g_1(x,Q^2)_{\rm LT} + g_1(x,Q^2)_{\rm HT}\,, \tag{1}$$

where "LT" denotes the leading twist ($\tau = 2$) contribution to g_1, while "HT" denotes the contribution to g_1 arising from QCD operators of higher twist, namely $\tau \geq 3$. The leading twist contribution reads:

$$\begin{aligned} g_1(x,Q^2)_{\rm LT} = g_1(x,Q^2)_{\rm pQCD} + h^{\rm TMC}(x,Q^2)/Q^2 \\ + \mathcal{O}(M^4/Q^4)\,, \end{aligned} \tag{2}$$

where, $g_1(x,\ Q^2)_{\rm pQCD}$ is the well-known NLO perturbative QCD contribution (logarithmic in Q^2) and for proton and neutron reads:

$$\begin{aligned} g_1(x,Q^2)_{\rm pQCD} = & \frac{1}{2}\sum_q^{n_f} e_q^2 \Bigg[(\Delta q + \Delta\bar{q}) \otimes \left(1 + \frac{\alpha_s(Q^2)}{2\pi}\delta C_q\right) \\ & + \frac{\alpha_s(Q^2)}{2\pi}\Delta G \otimes \frac{\delta C_G}{n_f}\Bigg], \end{aligned} \tag{3}$$

and also the spin dependent deuteron structure function $xg_1^d(x,\ Q^2)$ can be represented in terms of the proton and neutron structure functions, $xg_1^p(x,\ Q^2)$ and $xg_1^n(x,\ Q^2)$ using the relation:

$$xg_1^d(x,Q^2) = \frac{1}{2}(1 - \frac{3}{2}\omega_D)[xg_1^p(x,Q^2) + xg_1^n(x,Q^2)], \tag{4}$$

where $\omega_D = 0.05 \pm 0.01$ is the D-state wave probability for the deuteron [28]. In Eq. (2), $h^{\rm TMC}(x,\ Q^2)$ stands for the exactly calculable kinematic target mass corrections [29–31] which being purely kinematic, effectively belong to the LT term. In Eq. (3), $\Delta q(x,\ Q^2)$, $\Delta\bar{q}(x,\ Q^2)$ and $\Delta G(x,\ Q^2)$ are the quark, antiquark and gluon polarized densities in the proton, respectively, which are evolved in Q^2 according to the spin-dependent NLO DGLAP equations. In Eq. (3), $\delta C(x)_{q,G}$ are the NLO spin-dependent Wilson coefficient functions and the symbol $\otimes$ denotes the usual convolution in Bjorken x-space. Moreover, n_f is the number of active quark flavors ($n_f = 3$ in our analysis).

In addition to the LT contribution, the following dynamical higher twist effects

$$g_1(x,Q^2)_{\rm HT} = h(x,Q^2)/Q^2 + \mathcal{O}(\Lambda^4/Q^4)\,, \tag{5}$$

must be taken into account at low Q^2 [27]. The latter are nonperturbative effects which cannot be calculated in a model independent way. That is why we prefer to extract them directly from the experimental data. This method is used to extract simultaneously the polarized parton densities and higher twist corrections to g_1. In the standard QCD analysis of DIS polarized structure function and to eliminate the nonperturbative effect, it is necessary to apply the appropriate cut for invariant-mass squard $W^2 = Q^2(1/x - 1) + M_N^2$. In fact choosing the appropriate W^2 cut is required to ignore the nonperturbative effects arising from higher twist dynamics.

3 Fitting contents in QCD analysis

The theory of QCD is responsible for justifying the structure of hadrons such as protons and neutrons. In this regard, the QCD analysis is a procedure to extract important information about the partonic structure of hadrons on the basis of experimental data. One important aspect of QCD analysis is fitting the experimental data with the theoretical predictions. Theoretical predictions are usually calculated in the framework of pQCD which involves a series expansion in the strong coupling constant $\alpha_s(Q^2)$. However, the perturbative expansions are just applied at high energies so at low energies the non-perturbative effects become important. Therefore, the data fitting requires the incorporation of both perturbative and non-perturbative effects. The fitting procedure involves an appropriate parameterization for the PDFs such as the case in determining the FFs [32–34]. It also includes the strong coupling constant. One commonly used parameterization is a series expansion in terms of orthogonal polynomials, such as the Gegenbauer polynomials. The coefficients of the polynomial expansion are determined by fitting the experimental data. The fitting procedure is often complicated by the presence of correlations between the various parameters, which can lead to large uncertainties in the

extracted values. Therefore, various techniques such as Monte Carlo simulations [35] and Bayesian methods [36] are used to estimate the uncertainties and to determine the best-fit values. In next section, we describe our QCD analysis of polarized DIS data to determine the spin structure function $g_1(x,\ Q^2)$.

4 QCD analysis of polarized deep inelastic scattering data for $xg_1(x, Q^2)$

4.1 Description of the data sets

In QCD analysis, the PDFs are determined by fitting theoretical predictions to experimental data from DIS processes, where a high-energy lepton beam is scattered off a hadronic target. The DIS data can provide main information on the structure functions of target which can be related to the PDFs. The fitting procedure operates by varying the free parameters in the theoretical calculations, including the ones in PDFs, to minimize a global chi-squared function, which measures the difference between the theoretical predictions and the experimental data. The best-fit PDFs are then used to make predictions for the production rates of various particles.

The QCD evolution of the PDFs is governed by the Dokshitzer-Gribov-Lipatov-Altarelli-Parisi [37–44] (DGLAP) equations, which describe how the PDFs evolve as the momentum transfer Q increases. The QCD analysis does typically involve the evolution of PDFs at next-to-leading order (NLO) accuracy, which includes one-loop corrections to the leading-order calculations. The analysis is also done in the framework of fixed-flavor-number scheme (FFNs) where the number of active partonic flavors is assumed to be constant throughout the evolution. The choice of renormalization (μ_R) and factorization (μ_F) scales which are related to the separation of short-distance and long-distance physics, is a key source of uncertainty in the analysis.

The QCD analysis is typically carried out using numerical programs that implement the theoretical calculations and perform the fitting procedure. One of these programs is the QCD-PEGASUS [45] which is employed in our analysis. This program uses a parameterization of the PDFs in Mellin-moment space, which allows for efficient numerical calculations. The program also includes the effects of NLO coupling constant, which is using a fourth-order Runge-Kutta integration.

The QCD analysis does also require a large amount of experimental data on DIS processes, which has been collected by various experiments at different colliders. In this paper we present a NLO QCD analysis of the word data set on the nucleon spin structure unction g_1^N (N=p,n and d) including the final JLAB **CLAS/EG1b** data on proton [56] and deuteron [57] spin structure function, see Table 1.

The QCD analysis is a complex and sophisticated method that requires a deep understanding of QCD and a careful treatment of experimental uncertainties. Since, the PDFs are essential tools for understanding the structure of hadrons then their accuracies are the key sources of uncertainties in many measurements in colliders. Therefore, determining of PDFs with as much accuracy as possible is an active area of research in particle physics.

4.2 χ^2 minimization

In this section, we describe the global analysis of the $xg_1(x,\ Q^2)$ data. We start by defining the χ^2-function which measures the goodness-of-fit between the experimental data and theoretical predictions. The χ^2 function is defined as:

$$\chi^2_{\text{global}} = \sum_n w_n \chi^2_n \,, \tag{6}$$

where, the sum involves different experiments and the relevant weight factor for the n^{th} experiment is denoted by w_n [64, 65]. The weight factors can be determined by physics considerations or other information as a prior knowledge. In our analysis, we take the weight factors to be unity. The χ^2_n-function for the n^{th} experiment has the following form:

$$\chi^2_n = \left(\frac{1-\mathcal{N}_n}{\Delta\mathcal{N}_n}\right)^2 + \sum_i \left(\frac{\mathcal{N}_n\, g^{exp}_{1,i} - g^{theor}_{1,i}}{\mathcal{N}_n\, \Delta g^{exp}_{1,i}}\right)^2 , \tag{7}$$

where $g^{exp}_{1,i}$ and $\Delta g^{exp}_{1,i}$ are the experimental value and its uncertainty for the i^{th} data point, and $g^{theor}_{1,i}$ is the theoretical prediction for the same data point. $\mathcal{N}_n$ is an overall normalization factor and $\Delta\mathcal{N}_n$ is the experimental normalization uncertainty for the data of n^{th} experiment. The normalization factor $\mathcal{N}_n$ is allowed to be shifted among different data sets considering the uncertainties $\Delta\mathcal{N}_n$ raised from various experiments. To estimate the uncertainties in the Polarized PDF parameters, we employed the Hessian method. In this approach, the fitted parameters are determined by the criterion $\Delta\chi^2 = T^2$. We select a tolerance parameter T such that this criterion guarantees that each dataset is described within the desired confidence level. The correlated statistical error for any quantity q_i is derived using standard error propagation techniques [66]:

$$(\sigma_{q_i})^2 = \Delta\chi^2 \left(\sum_{\alpha,\beta} \frac{\partial q_i}{\partial p_\alpha} C_{\alpha,\beta} \frac{\partial q_i}{\partial p_\beta}\right) . \tag{8}$$

Table 1 The summary of data sets for polarized DIS structure function used in our analysis with measured x and Q^2 ranges, including the number of data points, individual χ^2 for each data set and total χ^2 for **Fit A** and **Fit B**

Experiment	Ref.	$[x_{\min}, x_{\max}]$	Q^2 (GeV^2)	Data poi.	χ^2_{FitA}	χ^2_{FitB}
SLAC/E143(p)	[46]	[0.031–0.749]	1.27–9.52	28	35.8489	30.2058
SMC(p)	[47]	[0.005–0.480]	1.30–58.0	12	9.6071	4.2217
EMC(p)	[48, 49]	[0.015–0.466]	3.50–29.5	10	5.9626	5.8783
SLAC/E155	[50]	[0.015–0.750]	1.22–34.72	24	24.6299	25.1583
HERMES06(p)	[51]	[0.0058–0.7311]	0.26–14.29	45	24.4420	20.5809
COMPASS10(p)	[52, 53]	[0.005–0.568]	1.10–62.10	15	25.7645	14.6390
COMPASS16(p)	[54]	[0.0035–0.575]	1.03–96.1	51	438.6187	34.5966
CLAS/EG1b(p)	[56]	[0.1212–0.5928]	1.0025–4.6474	166	188.2738	100.4762
$\mathbf{g_1^p}$				**351**	**353.1475**	**235.7568**
SLAC/E143(d)	[46]	[0.031–0.749]	1.27–9.52	28	50.7407	41.7123
SLAC/E155(d)	[62]	[0.015–0.750]	1.22–34.79	24	23.8881	18.5615
SMC(d)	[47]	[0.005–0.479]	1.30–54.80	12	20.5320	18.3085
HERMES06(d)	[51]	[0.0058–0.7311]	0.26–14.29	45	46.9611	34.7242
COMPASS17(d)	[63]	[0.0045–0.569]	1.03–74.1	43	32.7938	28.6343
CLAS/EG1b(d)	[57]	[0.121–0.5925]	1.0022–4.647.1	158	238.7377	170.9141
$\mathbf{g_1^d}$				**310**	**413.6533**	**312.8549**
SLAC/E142(n)	[60]	[0.035–0.466]	1.10–5.50	8	3.0421	11.7568
HERMES(n)	[61]	[0.033–0.464]	1.22–5.25	9	2.3284	4.3302
E154(n)	[58]	[0.017–0.564]	1.20–15.00	17	16.2231	4.1086
JLAB-Hall A(n)	[59]	[0.33–0.60]	2.71–4.8	3	6.2181	13.7721
$\mathbf{g_1^n}$				**29**	**27.8117**	**33.9676**
Total	**690**				**805.4552**	**582.5740**
$\chi^2/d.o.f$	–				**1.1523**	**0.8747**

By considering the Hessian matrix as $H_{\alpha,\beta} = \frac{1}{2}\partial^2\chi^2/\partial p_\alpha \partial p_\beta$, one can find that the covariance matrix $C = H^{-1}$ is the inverse of the Hessian matrix, evaluated at the χ^2 minimum. To compute the fully correlated 1σ error bands corresponding to 68% confidence level for Polarized PDFs, one can choose $T = 1$. To determine the unknown parameters in our theoretical model, we minimize the χ^2_{global}-function using the CERN program library MINUIT [67]. The unknown parameters might initially include the strong coupling constant at the initial energy scale, $\alpha_s(Q_0^2)$.

5 Global analysis

5.1 Fitting function

The spin dependent PDFs have been investigated so far in pQCD utilizing different functional forms [14, 15, 17–19, 21, 22, 27, 69–82, 87, 88]. To perform the relevant global fit for the polarized PDFs, a convenient parameterized form is usually used to model the PDFs at the initial energy scale $Q_0^2 = 1$ GeV^2. It should also be noted that the choice of functional form of PDFs is not unique and various parameterizations can lead to different results. Therefore, it is important to perform a thorough analysis with various parameterizations to assess the reliability of extracted PDFs [89, 90]. Through this work, we use the Gegenbauer polynomials to parameterize the polarized PDFs, which is a common choice in modern global analyses. These polynomials are a basis set for functions on the interval $[-1, 1]$ and can be used to expand the parton distributions as a series. The expansion coefficients are then the free parameters in the fit. The advantage of using the Gegenbauer polynomials is that they allow for a systematic way of including higher twist contributions in the analysis, as well as a more flexible functional form compared to the traditional DGLAP evolution approach. Additionally, the Gegenbauer moments can be related to physical observables such as the axial charge of the nucleon, which provides a direct connection to QCD. From now on, we adopt the following form for the PDFs:

$$\Delta q\left(x, Q_0^2\right) = \mathcal{N}_q \eta_q x^{\alpha_q} (1-x)^{\beta_q} \left(\sum_{i=0}^{2} a_i^q C_i^{15/2}(1-2x)\right). \tag{9}$$

Here, Second-order Gegenbauer polynomials are used instead of simple second-order polynomials because they are orthogonal with respect to the weight function $x^\alpha(1-x)^\beta$, which reflects the typical shape of PDFs. This orthogonality reduces correlations among expansion coefficients, resulting in more stable and efficient approximations. Additionally, Gegenbauer polynomials provide

faster and more uniform convergence across the entire domain, especially near the endpoints x=0 and x=1. They also help reduce oscillations near boundaries (Runge's phenomenon), improving the quality of the approximation compared to simple polynomials of the same order and the parameters η_q are defined as the first moments of the polarized parton distribution functions (PPDFs), representing the net spin contribution of parton flavor q to the nucleon spin:

$$\eta_q = \int_0^1 dx \Delta q_j(x, Q_0^2). \tag{10}$$

Since η_q are fixed physical quantities determined from theory, sum rules, or experimental constraints the normalization constants $\mathcal{N}_q$ are chosen to ensure that the parameterized PPDFs satisfy this moment condition. For a PPDF parameterized as

$$x\Delta q(x, Q_0^2) = \mathcal{N}_q\, \eta_q\, x^{\alpha_q}(1-x)^{\beta_q} \left(\sum_{i=0}^{2} a_i^q C_i^{15/2}(1-2x)\right) \tag{11}$$

the normalization constant $\mathcal{N}_q$ is computed by imposing

$$\eta_q = \mathcal{N}_q \int_0^1 dx x^{\alpha_q}(1-x)^{\beta_q} \left(\sum_{i=0}^{2} a_i^q C_i^{15/2}(1-2x)\right). \tag{12}$$

which yields

$$\mathcal{N}_q = \frac{\eta_q}{\int_0^1 dx x^{\alpha_q}(1-x)^{\beta_q} \left(\sum_{i=0}^{2} a_i^q C_i^{15/2}(1-2x)\right)}. \tag{13}$$

In this framework, the shape parameters α, β and a_i^q define the functional form of the PPDF, while $\mathcal{N}_q$ rescales it so that the first moment matches the physical input η_q. Thus, η_q serves as a physical constraint, and $\mathcal{N}_q$ is determined accordingly. The normalization factors $\mathcal{N}_q$ is determined as:

$$\begin{aligned}\frac{1}{\mathcal{N}_q} =& \frac{\gamma(\alpha_q)\gamma(\beta_q+1)}{\gamma(\alpha_q+\beta_q+3)}\Big\{30a_2^q\Big[-\alpha_q(9\beta_q+5)+4\alpha_q^2+4(\beta_q+1)(\beta_q+2)\Big] \\ &+(\alpha_q+\beta_q+2)\Big[a_0^q(\alpha_q+\beta_q+1)-15a_1^q(\alpha_q-\beta_q-1)\Big]\Big\}.\end{aligned} \tag{14}$$

In Eq. (9), Δq stands for the general form of PDFs, i.e., Δu_v, Δd_v, $\Delta\bar{q}$, and Δg represent the individual polarized up-valence, down-valence, sea and gluon distributions, respectively and the Gegenbauer polynomials $C_i^{15/2}(1-2x)$ are a family of orthogonal polynomials that can be defined by a generating function. The generating function of the Gegenbauer polynomials is a power series that represents a function in terms of its derivatives. Specifically, the generating function of the Gegenbauer polynomials is given by [91]:

$$\frac{1}{(1-2xt+t^2)^{\lambda}} = \sum_{n=0}^{\infty} C_n^{\lambda}(x)t^n\,, \tag{15}$$

where λ is a real number and $C_n^{\lambda}(x)$ is the n^{th} Gegenbauer polynomial of degree λ. In the specific given equation, $C_i^{15/2}(1-2x)$ is a Gegenbauer polynomial of degree 15/2 evaluated at the argument $1-2x$. The parameter λ controls the scaling or domain mapping in the Gegenbauer polynomial expansion. It effectively sets the "length scale" to optimize the polynomial basis for approximating the target function. The specific choice $\lambda = \frac{15}{2}$ is motivated by numerical tests and theoretical considerations aimed at minimizing approximation errors, particularly at large x, thereby improving the overall fit quality. This polynomial appears in a mathematical expression that likely involves some sort of special function or mathematical operation,

$$\begin{aligned}C_0^{\lambda}(x) =& 1 \\ C_1^{\lambda}(x) =& 2\lambda x \\ C_2^{\lambda}(x) =& -\lambda + 2\lambda(1+\lambda)x^2 \\ C_3^{\lambda}(x) =& -2\lambda(1+\lambda)x + \frac{4}{3}\lambda(1+\lambda)(2+\lambda)x^3\,.\end{aligned} \tag{16}$$

A recursive relation in Gegenbauer polynomials is presented as:

$$nC_n^{\lambda}(x) = 2(n+\lambda-1)xC_{n-1}^{\lambda}(x) - (n+2\lambda-2)C_{n-2}^{\lambda}(x) \tag{17}$$

It should be noted that, the polarized PDFs given in Eq. (9) are satisfied the positivity constrain. At LO, this constrain implies:

$$|\Delta q(x, Q_0^2)| \leq q(x, Q_0^2),\ |\Delta\bar{q}(x, Q_0^2)| \leq \bar{q}(x, Q_0^2), \tag{18}$$

which are the direct consequent of a probabilistic interpretation of the parton distribution in the naive parton model. On the other hand, in the absence of charm and bottom quark contributions and without SIDIS data, the analysis assumes the SU(3) flavor

symmetry, which implies that the polarized distributions of $\bar{u}$, $\bar{d}$, $\bar{s}$, and s are equal at the initial scale Q_0^2 so are denoted by $\Delta\bar{q}$. This assumption reduces the number of free parameters in the fit. More complicated constrains appear in approximations beyond the leading order QCD.

It is worth noting that, in Eq. (9) the two free parameters $\mathcal{N}_q$ and η_q are not independent and there is a relation between these two parameters. In fact, η_q represents the first moments of $\Delta q_i(x,\ Q_0^2)$ which is given by $\eta_i = \int_0^1 dx\ \Delta q_i(x,\ Q_0^2)$. This relation can be used as a constraint in the global fit which reduces the number of free parameters and improves the stability of the fit.

In order to perform the global QCD fit of the polarized DIS data, the total number of free parameters for each of the four type components is six, yielding a total of 24 degrees of freedom, see Eq. (9). However, some of these parameters are fixed in advance and discarded in the fit to reduce the number of free parameters. In particular, the first moments of the polarized valence distributions are fixed using the axial charges for octet baryon F and D, measured in hyperon and neutron β decay. This yields the numerical values of $\eta_{u_v} = 0.928 \pm 0.014$ and $\eta_{d_v} = -0.342 \pm 0.018$ [92], which are then fixed to their central values. The parameters $\eta_{\bar{q}}$ and η_g are determined through the fit.

5.2 Mellin moment space for $\mathbf{xg_1(x,\ Q^2)}$

After defining the parameters and their status, the next step is to determine them through the fitting procedure. This can be done by performing the necessary computations in the Mellin moment space. The Mellin transform of the structure function $g_1(x,\ Q^2)$ is expressed by the following equation:

$$\mathcal{M}_1^{\mathrm{N}}(Q^2) \equiv \int_0^1 dx\, x^{\mathrm{N}-1}\, g_1(x, Q^2)\,. \tag{19}$$

In this space, the moment of the polarized structure function $\mathcal{M}_1^{\mathrm{N}}(Q^2)$ for the proton at the twist-2 contribution can be expressed in terms of polarized PDFs and the coefficient functions ΔC_i^N as follows [93]:

$$\begin{aligned}\mathcal{M}_1^{\mathrm{N,p}}(Q^2) =& \frac{1}{2}\sum_q e_q^2 \Big\{(1+\frac{\alpha_s}{2\pi}\Delta C_q^N)\\ &\times[\Delta q(N,Q^2)+\Delta\bar{q}(N,Q^2)]\\ &+\frac{\alpha_s}{2\pi}\,2\Delta C_g^N\,\Delta g(N,Q^2)\Big\}.\end{aligned} \tag{20}$$

In this equation, the sum runs over the quark flavors u, d, s. Also $\Delta q(N,\ Q^2)$, $\Delta\bar{q}(N,\ Q^2)$ and $\Delta g(N,\ Q^2)$ denote the polarized quark, anti-quark and gluon distributions in Mellin N-space, respectively, which are obtained by a similar transform as Eq. (19). It is important to mention that Δq is defined here as $\Delta q = \Delta q_v - \Delta\bar{q}$. Finally, ΔC_i^N represent the polarized Wilson coefficients in Mellin space which are given by [93]:

$$\begin{aligned}\Delta C_q^N =& \frac{4}{3}\Big\{-S_2(N)+(S_1(N))^2+\Big(\frac{3}{2}-\frac{1}{N(N+1)}\Big)\\ &\times\ S_1(N)+\frac{1}{N^2}+\frac{1}{2N}+\frac{1}{N+1}-\frac{9}{2}\Big\},\end{aligned} \tag{21}$$

and

$$\Delta C_g^N = \frac{1}{2}\Big[-\frac{N-1}{N(N+1)}(S_1(N)+1)-\frac{1}{N^2}+\frac{2}{N(N+1)}\Big], \tag{22}$$

with $S_1(n) = \sum_{j=1}^n (1/j) = \psi(n+1)+\gamma_E$, $S_2(n) = \sum_{j=1}^n (1/j^2) = \pi^2/6 - \psi'(n+1)$, $\psi(n) = \Gamma'(n)/\Gamma(n)$ and $\psi'(n) = d^2\ln\Gamma(n)/dn^2$. Now, the moment of polarized structure function, i.e. $\mathcal{M}_1^{\mathrm{N,n}}(Q^2)$, at the twist-2 contribution can be written similarly for the neutron in terms of the coefficient functions ΔC_i^N and polarized PDFs as:

$$\begin{aligned}\mathcal{M}_1^{\mathrm{N,n}}(Q^2) =& \mathcal{M}_1^{\mathrm{N,p}}(Q^2) - \frac{1}{6}\Big(1+\frac{\alpha_s}{2\pi}\Delta C_q^N\Big)\\ &\times\ \big(\Delta u_v(N,Q^2)-\Delta d_v(N,Q^2)\big).\end{aligned} \tag{23}$$

Then the deuteron structure function can be related to the proton and neutron ones as follows:

$$\mathcal{M}_1^{\mathrm{N,d}}(Q^2) = \frac{1}{2}\Big(\mathcal{M}_1^{\mathrm{N,p}}(Q^2)+\mathcal{M}_1^{\mathrm{N,n}}(Q^2)\Big)\times\Big(1-\frac{3}{2}\omega_D\Big). \tag{24}$$

In this equation, $\omega_D = 0.05 \pm 0.01$ denotes the $D-$state wave probability for the deuteron [94, 95]. Now, using Eq. (20) and the experimental data on the polarized structure function g_1^p one can perform a global fit to extract unknown parameters. The global fit involves a comparison between the experimental data for the polarized structure function and their theoretical predictions including free parameters. These parameters are adjusted somehow a best fit is obtained. This procedure is known as a "global analysis" or

Table 2 The value of free parameters and their statistical errors in the $\overline{\text{MS}}$ scheme at the initial scale $Q_0^2 = 1$ GeV^2 for **Fit A** and **Fit B**

		Fit A	Fit B
Δu_v	η_{u_v}	0.9280(Fixed)	0.9280(Fixed)
	α_{u_v}	0.135565 ± 0.016970	0.117902 ± 0.003922
	β_{u_v}	1.075346 ± 0.059691	1.360279 ± 0.046427
	$a_0^{u_v}$	140.428163 ± 7.420826	144.467555 ± 0.232128
	$a_1^{u_v}$	4.192738 ± 0.458763	3.347560 ± 0.015801
	$a_2^{u_v}$	-1.643730 ± 0.069709	-1.650575 ± 0.001980
Δd_v	η_{d_v}	-0.342(Fixed)	-0.342(Fixed)
	α_{d_v}	1.000000 ± 0.005093	0.755056 ± 0.034417
	β_{d_v}	4.896196 ± 0.487310	2.997030 ± 0.293166
	$a_0^{d_v}$	112.480969 ± 54.172578	213.168050 ± 43.870856
	$a_1^{d_v}$	3.023899 ± 2.568452	9.951375 ± 6.606230
	$a_2^{d_v}$	0.0(Fixed)	0.0(Fixed)
$2(\Delta\bar{u} + \Delta\bar{d})$	$\eta_{\bar{q}}$	-2.421468 ± 1.044638	-0.134663 ± 0.007655
	$\alpha_{\bar{q}}$	0.036875 ± 0.006505	2.080387 ± 0.114363
	$\beta_{\bar{q}}$	37.510597 ± 1.226059	5.306717 ± 0.304069
	$a_0^{\bar{q}}$	350.355761 ± 1.229773	-989.871050 ± 0.948004
	$a_1^{\bar{q}}$	4.811529 ± 1.229770	72.195650 ± 0.946040
	$a_2^{\bar{q}}$	6.338840 ± 1.229805	-10.201256 ± 0.849316
Δg	η_g	0.119032 ± 0.053216	0.166831 ± 0.050151
	α_g	21.273566 ± 1.126319	20.119238 ± 21.822621
	β_g	40.303285 ± 2.226121	37.723573 ± 13.731742
	a_0^g	-17.766035 ± 13.863802	-5.658637 ± 2.816638
	a_1^g	49.827550 ± 14.309688	33.359421 ± 6.090680
	a_2^g	1.011844 ± 6.452208	1.136815 ± 2.245216
		$\alpha_s(Q_0^2) = 0.3834$(Fixed) $\alpha_s(M_Z^2) = 0.116032$	$\alpha_s(Q_0^2) = 0.3382$(Fixed) $\alpha_s(M_Z^2) = 0.116032$

"global fit" which is a standard technique used in extracting parton distribution functions. With respect to some constrains, we have finally 21 unknown parameters, embedded in the polarized parton distribution functions (Δq_v, $\Delta\bar{q}$, and Δg at the initial scale $Q_0^2 = 1$ GeV^2). Table 2 lists the numerical values of these parameters which we obtain during the fitting procedure. In next subsection a method which yield us the polarized parton densities in Bjorken x-space is discussed.

5.3 Inverse Mellin in moment space

In polarized physics, the inverse Mellin transform from moment space is a mathematical operation used to obtain a polarized PDF from its moments. The polarized PDF describes the probability density of finding a parton with a certain momentum fraction and spin within a polarized proton. The moments of polarized PDF can be defined as integrals of the PDF multiplied by a power of the momentum fraction x. Specifically, the n^{th} moment of the $g_1(x,\ Q^2)$ is given by Eq. (19). The inverse Mellin transform from moment space relates the polarized PDF $g_1(x,\ Q^2)$ to its moments $\mathcal{M}_1^{\mathrm{N}}(Q^2)$ through the following equation:

$$g_1(x, Q^2) = \frac{1}{\pi}\int_0^\infty dz\ Im[e^{i\phi}x^{-\mathrm{N}}\mathcal{M}_1^{\mathrm{N}}(Q^2)] \tag{25}$$

where, $\mathrm{N} = c + ze^{i\phi}$ and c is a constant that lies to the right of all singularities of the integrand. For all practical purposes one may choose $c \approx 1$, $\phi = 135°$ and an upper limit of integral as $5 + 10/lnx^{-1}$ (for any Q^2) instead of $z = \infty$ which suffices to guarantee the accurate and stable numerical results [96, 97].

The inverse Mellin transform, Eq. (25), is a powerful tool in polarized physics because it allows one to determine the polarized PDF from its moments, which can be calculated from experimental data or from theoretical calculations. By inverting the Mellin transform, one can obtain a detailed picture of the spin structure of the proton and deep insights into the dynamics of strong interactions.

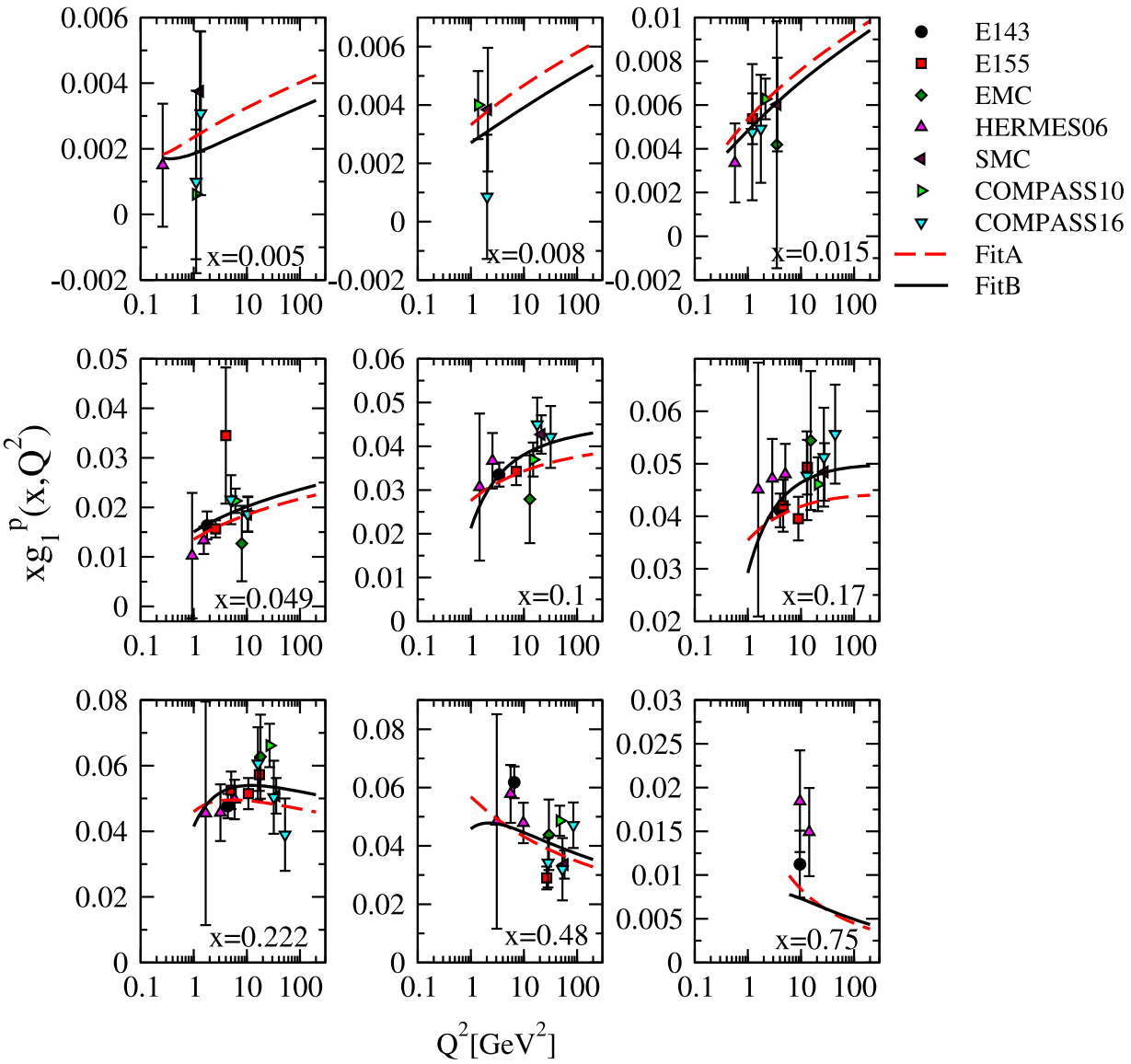

Fig. 2 Polarized proton structure function, $xg_1^p(x,\ Q^2)$, as a function of Q^2 at several x values in comparison to the experimental data of E143 [46], E155 [50], EMC [48, 49], HERMES06 [51], SMC [47], COMPASS10 [52, 53] and COMPASS16 [54]

5.4 Result of QCD fit

We use the data sets reported in Table 1 to do our analysis. This table lists the detailed information and references of data sets along with the kinematic range of x and Q^2. To start, we will divide our analysis in two main steps. In the first step (which is called as **Fit A**) we perform a fit with all 690 data points reported in Table 1 adopting the positivity constrains. We then include the higher twist (HT) effects on proton, neutron, and deuteron polarized structure functions. From now on this procedure is called **Fit B**. Since the **Fit B** contains all essential constraints, we will then use this for comparing in all tables and figures.

In Table 1, the values of individual χ^2 for each data set and total χ^2 for **Fit A** and **Fit B** are also listed. According to the results in Table 1, in **Fit A** by considering the positivity constrain and ignoring any higher twist correction, the total value of $\chi^2/d.o.f$ is 1.15. For a more complete discussion, including the positivity constrain and higher twist corrections in the fit would be necessary. In the second step, we obtain the total $\chi^2/d.o.f\ =\ 0.8747$ in **Fit B**. We are motivated to present **Fit A** and **Fit B** to show the necessity of including the HT corrections in the present QCD analysis. Obviously, in comparing between **Fit A** and **Fit B** there are improvements around 24% in the total χ^2. Moreover, a modification about 33% and 24% is obtained for the proton and deuteron's χ^2, respectively.

Some studies have indicated that to eliminate non-perturbative effects arising from higher twists, the standard $W^2 \geq 6.25$ GeV^2 cut is used to avoid the presence of dynamical higher twists effect [98]. Given the definition of the invariant mass squared, as shown

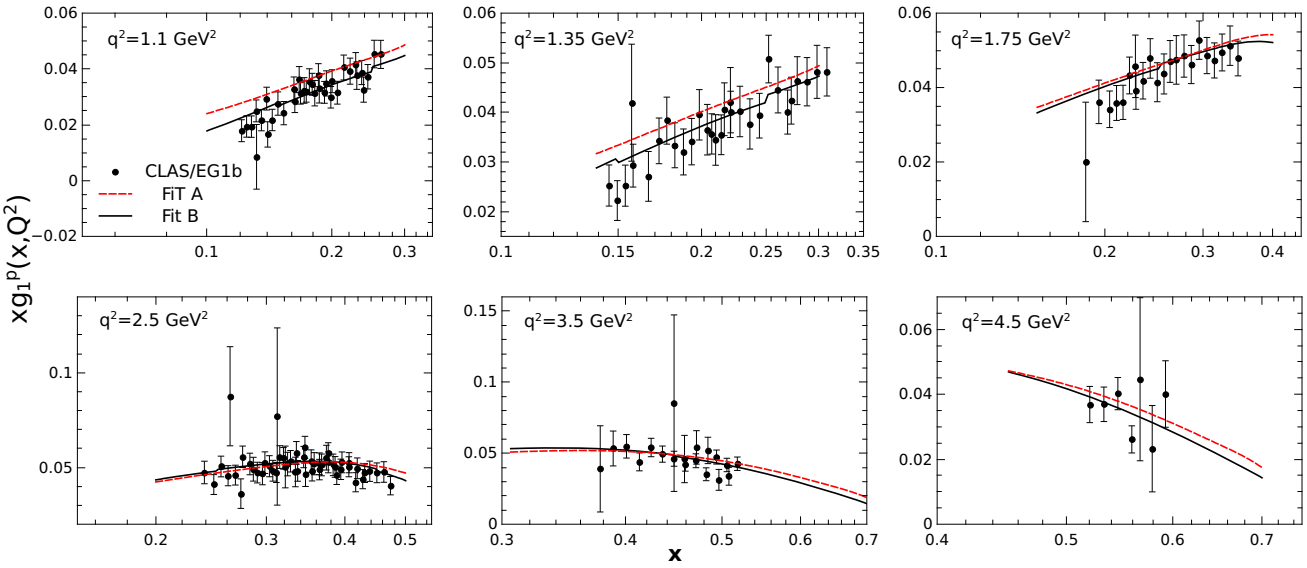

Fig. 3 Polarized proton structure function, $xg_1^p(x,\ Q^2)$, as a function of x at several Q^2 values in comparison to **JLAB CLAS/EG1b** experimental data [56]

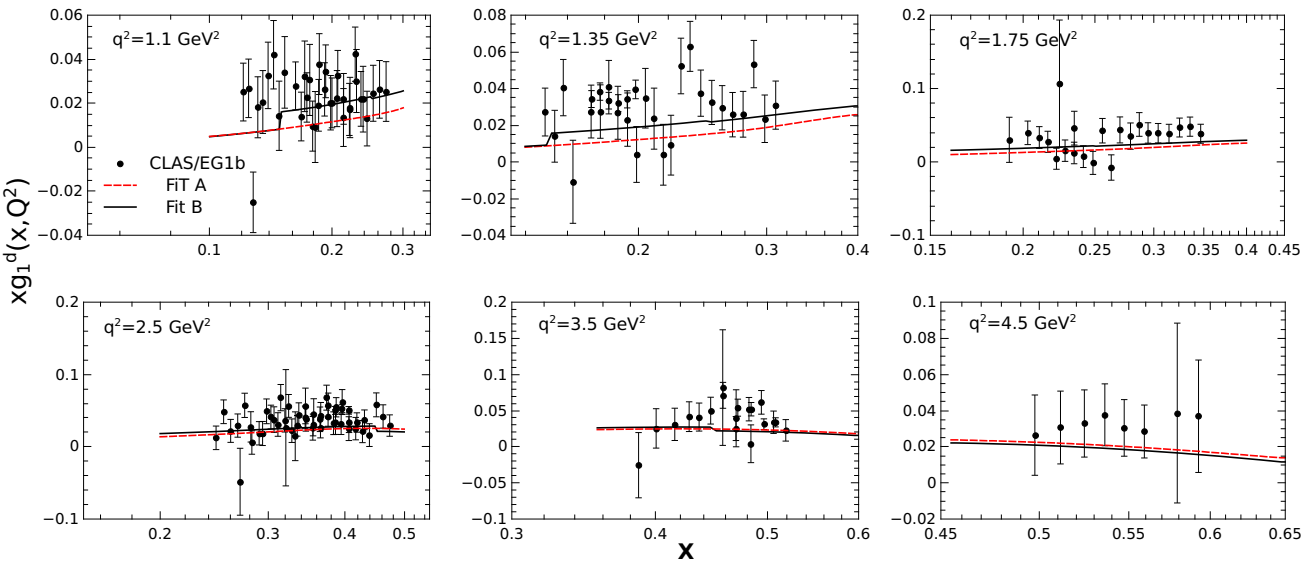

Fig. 4 Polarized deuteron structure function, $xg_1^d(x,\ Q^2)$, as a function of x at several Q^2 values in comparison to **JLAB CLAS/EG1b** experimental data [57]

in Fig. 1, from 324 data points related to the polarized structure function from **JLAB CLAS/EG1b** for proton and deuteron a considerable number of these data points located in a region where higher twist effects are significant. Therefore, accounting for these effects is expected to have a meaningful impact on these data. As shown in Table 1, incorporating higher twist effects results in an improvement in the fit quality by approximately 24% improvement compared to the **Fit A**. Most of this enhancement is attributed to the **JLAB CLAS/EG1b** for proton and deuteron data, with about 47% and 28% improvement in individual χ^2 for proton and deuteron data respectively.

In Table 2, the final values of fit parameters (in Eq. (9)) are summarized for the **Fit A** and **Fit B** at the initial scale $Q_0^2 = 1$ GeV^2. We find that, as earlier mentioned, including HT effects could improve the fit quality around 24%. In Table 3, the values of higher twist corrections extracted from the data in a model independent scheme at the initial scale $Q_0^2 = 1$ GeV^2 are presented.

We will begin by comparing the polarized structure functions for proton, neutron, and deuteron as this is the primary input to our fit. In Figs. 2, 3, 4, 5 and 6 we display the comparison of our Fits A and B with proton deuteron and neutron data used in this analysis.

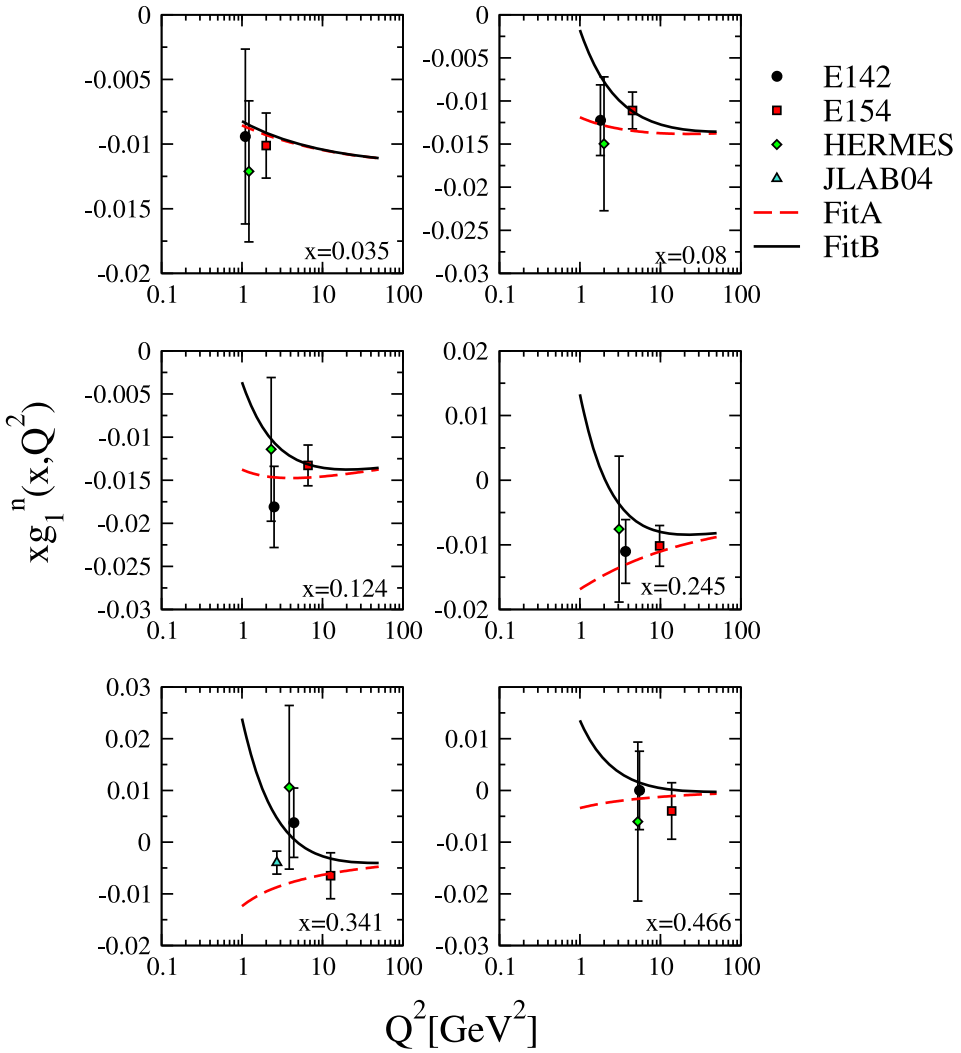

Fig. 5 Polarized neutron structure function, $xg_1^n(x,\ Q^2)$, as a function of Q^2 at several x values in comparison to experimental data of E142 [60], E154 [58], HERMES [61] and JLAB04 [59]

Table 3 The values of higher twist corrections extracted from the data in a model independent scheme at the initial scale $Q_0^2 = 1$ GeV^2

Fit B		
$< x_i >$	$h^p(x_i)[GeV^2]$	$h^n(x_i)[GeV^2]$
0.003–0.058	$8.95010097 \times 10^{-5}$	3.2093323×10^{-4}
0.05–0.15	$-1.1873577 \times 10^{-2}$	1.013764×10^{-2}
0.15–0.25	$-1.3140258 \times 10^{-2}$	3.014504×10^{-2}
0.25–0.45	$-1.1253071 \times 10^{-2}$	3.628907×10^{-2}
0.45–0.75	$-1.4101965 \times 10^{-2}$	1.696815×10^{-2}

In Fig. 2 for Fit A and B, the theoretical prediction are entirely consistent with the experimental data. It seems that no significant differences is observed for Fit A and B , indicating that including higher-twist correction does not have a substantial impact on the fit quality in the polarized proton structure function (except for the data from **CLAS/EG1b**)

To see the impact of inclusion of the higher-twist correction, Figs. 3 and 4 display the comparison of our fits with the data from **CLAS/EG1b**.

By comparing Fit A and B, although both theoretical prediction contained within the band of the experimental uncertainties, differences are observed in theoretical prediction extracted from Fit A and B within the kinematic range of the **CLAS/EG1b** data. These differences arise from the inclusion of the higher-twist correction.

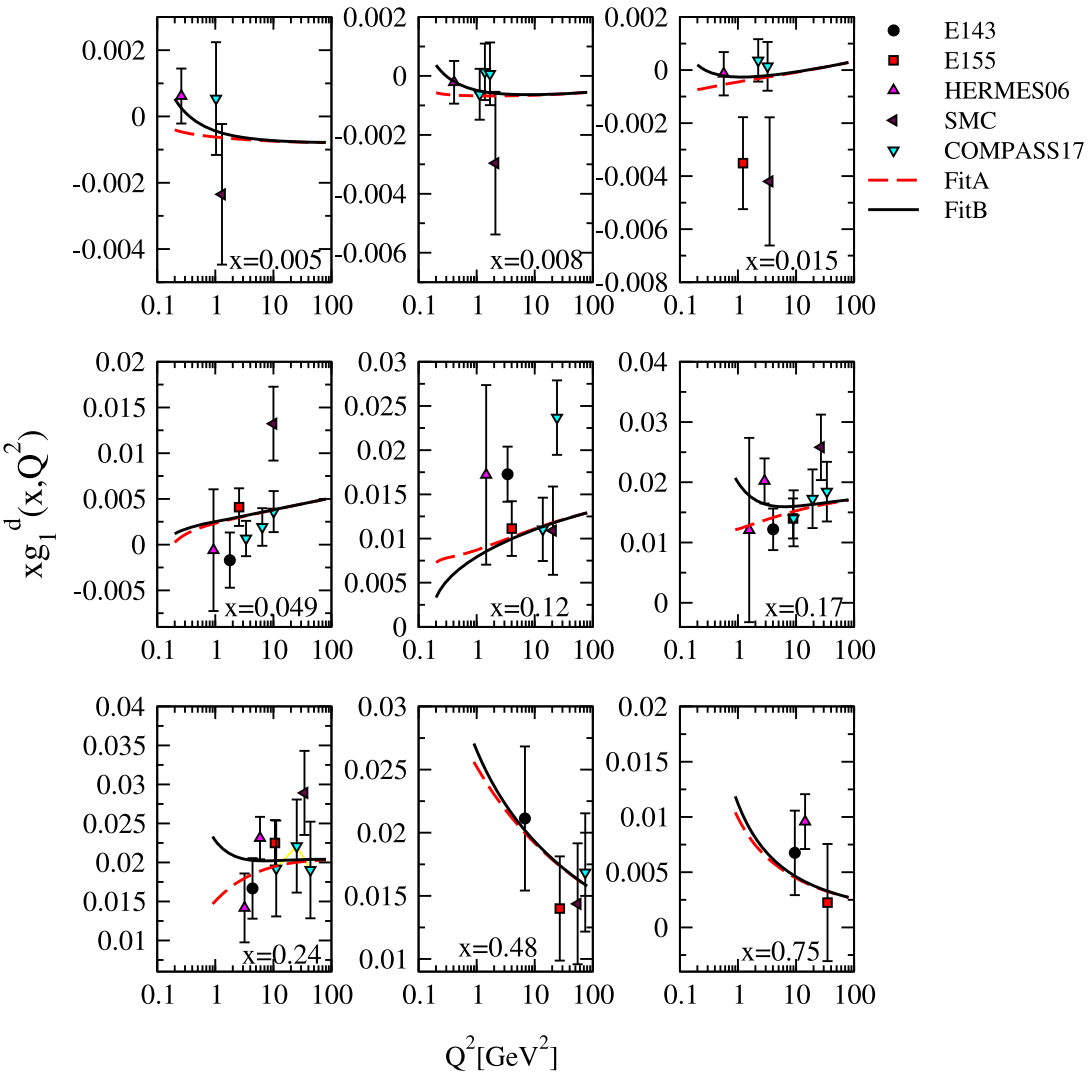

Fig. 6 Polarized deuteron structure function, $xg_1^d(x,\ Q^2)$, as a function of Q^2 at several x values in comparison to the experimental data of E143 [46], E155 [62], HERMES06 [51], SMC [47] and COMPASS17 [63]

As previously mentioned and also evident in these figures, including higher-twist correction lead to 47% and 28% improvement in the proton and deuteron χ^2 for **CLAS/EG1b** data. A clear consistency between the theoretical prediction and experimental data is observed in the regions of large x and low Q^2 for Fit B, where the nonperturbative effects such as higher-twist correction are significant and can not be neglect.

The differences between Fits A and B are also observed in the Fig. 5, where we compared our theoretical prediction with the neutron experimental data.

The observed difference between Fits A and B for the neutron structure function, compared to proton and deuteron, arises despite limited neutron data in the higher-twist sensitive kinematic region. This can be attributed to the neutron's distinct quark composition and greater sensitivity to higher-twist effects. Additionally, the deuteron, as a proton-neutron bound state, exhibits partial averaging of these effects, reducing visible differences. Limited neutron data and possible isospin symmetry breaking may also contribute to the pronounced impact of higher-twist corrections in the neutron analysis.

We also show the comparison of the theoretical prediction with experimental data for deuteron in Fig. 6. Same as Fig. 2, for Fit A and B, we find the theoretical prediction are entirely consistent with the experimental data. There is no significant differences is observed for Fit A and B , indicating that including higher-twist correction does not have a substantial impact on the fit quality in the polarized deuteron structure function (except for the data from **CLAS/EG1b**). We also compared our results with other parametrization models NAAMY [82], NMA23 [82], KATAO [22], as well as the data sets from E143 [46], JLAB CLAS/EG1b [56, 57], E154 [58] and COMPASS [54].

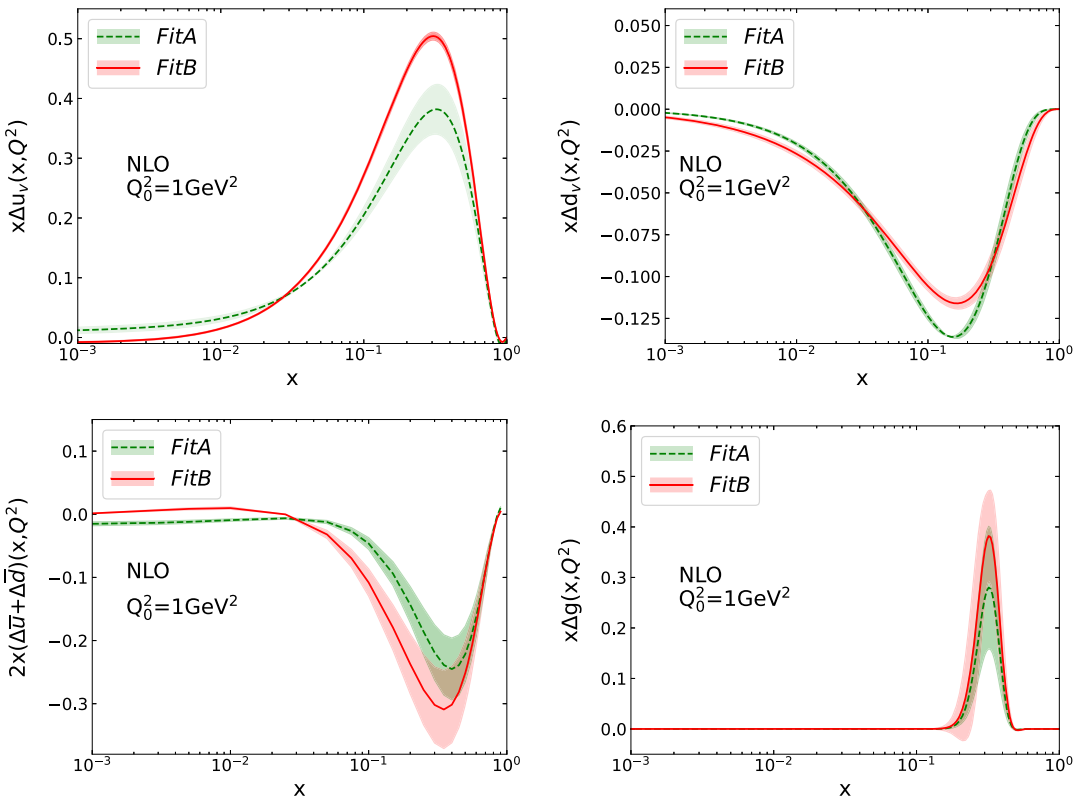

Fig. 7 The NLO polarized parton densities as a function of x at the initial scale $Q_0^2 = 1$ GeV^2 for **Fit A** and **Fit B**

Table 4 Our NLO results for the Bjorken sum rule, Γ_1^{NS}, Γ_1^p, Γ_1^n and Γ_1^d at NLO at $Q^2 = 3$ GeV^2 compared with the data from E143 [46], COMPASS16 [54] and COMPASS17 [55]

	E143 [46]	COMPASS16 [54]	COMPASS17 [55]	Fit B
Γ_1^{NS}	0.164 ± 0.023	0.181 ± 0.008	$0.192 \pm 0.007 \pm 0.015$	0.19375186 ± 0.0007610
Γ_1^{p}	0.133 ± 0.010	$0.139 \pm 0.003 \pm 0.009$		0.1503084 ± 0.0005041
Γ_1^{n}	-0.032 ± 0.018	$-0.041 \pm 0.006 \pm 0.011$		$-0.04344337 \pm 0.0012651$
Γ_1^{d}	0.047 ± 0.007	_	$0.043 \pm 0.001 \pm 0.003$	0.04878392 ± 0.0008076

In Fig. 7, we plot the extracted polarized PDFs at NLO accuracy as a function of x at the initial scale $Q_0^2 = 1$ GeV^2, using **Fit A** and **Fit B**. It is seen that the inclusion of higher twist (HT) affects the shapes and errors of the polarized PDFs. In all figures going forward, only results from **Fit B**, which accounts for the higher twist effect, will be presented due to its priority.

We present in Fig. 8 a comparison of our findings on polarized PDFs at $Q^2 = 2.5$ GeV^2 with the BB10 [78] and NMA23 [88] models. A significant reduction in the error band of the polarized density is observed for the **Fit B**, compared to other models.

As shown, Fit B shows smaller error bands compared to other analyses because they reflect only statistical uncertainties from data propagated via the Hessian method within our Gegenbauer polynomial parametrization. This approach, combined with recent high-precision data and stricter cuts, reduces uncertainties but does not include other sources such as model assumptions or scale variations. Thus, these bands represent statistical precision but not the full uncertainty. Differences with other results also arise from methodological choices.

To show the consistency of our model to the other polarized structure functions, we also calculate the $g_2^p(x,\ Q^2)$ structure function via the Wandzura-Wilczek relation [83, 84]:

$$g_2(x, Q^2) = -g_1^p(x, Q^2) + \int_x^1 \frac{dy}{y} g_1^p(y, Q^2)\,. \tag{26}$$

Fig.9 shows the polarized $g_2^p(x,\ Q^2)$ structure function as function of x for **Fit B**, compared to the E155 datasets and other parameterization model such as KTA17 [21] and NMA23 NLO [82].

Our findings align well with existing data and parametrization models, suggesting a successful prediction has been made.

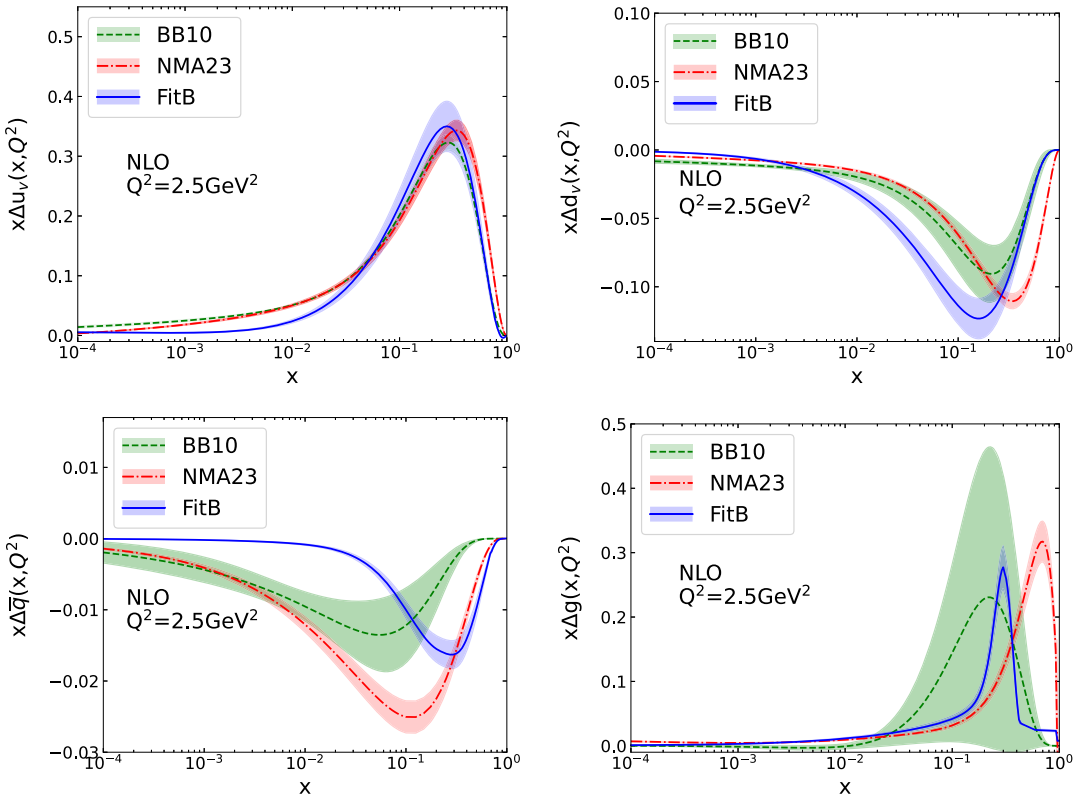

Fig. 8 Polarized parton densities at $Q^2 = 2.5$ GeV^2 in **Fit B** which are compared with BB10 [78] and NMA23 [88] models

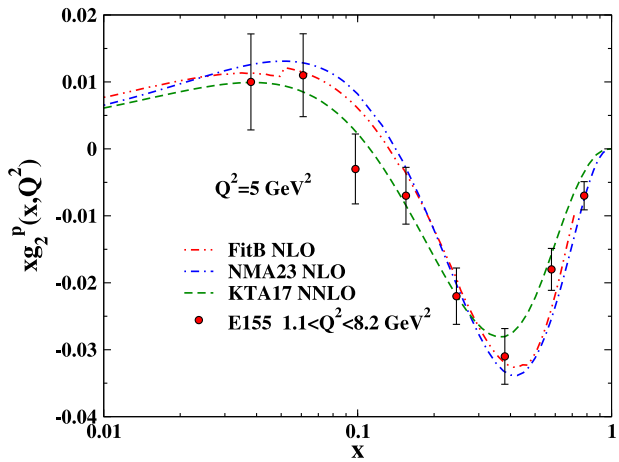

Fig. 9 The spin dependent structure functions xg_2 of proton at the energy scales $Q^2 = 5$ GeV^2. The results of **Fit B** (dash-dotted-dotted line) at NLO accuracy is compared with the parametrization models like KTA17 (dashed line) [21] and NMA23 NLO (dash-dotted line) [82]

6 Bjorken sum rule and proton helicity sum rule

In order to confirm the accuracy of fitting results, we can calculate several sum rules. These sum rules provide a consistency check on the fitted PDFs by relating integrals of the PDFs to known physical quantities. In this section, we demonstrate the calculation of these sum rules and show how they can be used to verify the quality of the PDF fits. The polarized Bjorken sum rule is obtained by integrating the spin distributions of quarks inside the nucleon over the Bjorken scale x. It provides a measure of the contribution of quark spins to the total spin of the nucleon. This sum can be expressed as a product of the nucleon axial charge g_A, which is measured in neutron β decay, and a coefficient function $C_{Bj}[\alpha_s(Q^2)]$. Taking into account the effects of HT corrections, the polarized Bjorken sum rule is given by the following equation [99]:

Table 5 The same as Table 4 at $Q^2 = 5$ GeV^2 compared with E143 [46], SMC [71], HERMES06 [51]. Only HERMES06 [51] results are not extrapolated in full x range (measured in region $0.021 \leq x \leq 0.9$)

	E143 [46]	SMC [71]	HERMES06 [51]	Fit B
Γ_1^{NS}	0.164 ± 0.021	0.181 ± 0.035	0.148 ± 0.017	0.19525107 ± 0.0006312
Γ_1^{p}	0.129 ± 0.010	0.132 ± 0.017	0.1211 ± 0.0092	0.1512962 ± 0.0005950
Γ_1^{n}	-0.034 ± 0.017	-0.048 ± 0.022	-0.0268 ± 0.0094	$-0.043954791 \pm 0.0012262$
Γ_{x1}^{d}	0.044 ± 0.007	0.039 ± 0.008	0.0436 ± 0.0035	$0.049001390 \pm 0.0008313$

Table 6 Results for the Bjorken sum rule, $\Gamma_1^{p,n,d}$ at the scales Q^2= 10, 50, 100 GeV^2 in the $\overline{\text{MS}}$ scheme in **Fit B**

$Q^2(GeV^2)$	Γ_1^p	Γ_1^n	Γ_1^d
10	0.1523868 ± 0.00068463	$-0.044525320 \pm 0.0011876$	$0.0492387707 \pm 0.000854$
50	0.1540998 ± 0.00080266	$-0.045458747 \pm 0.0011347$	$0.0495946627 \pm 0.00088442$
100	0.1546254 ± 0.00083342	$-0.045756355 \pm 0.0011203$	$0.0496987301 \pm 0.00089189$

Table 7 First moments of the polarized structure functions Γ_1^p ,Γ_1^d, Γ_1^n at $Q^2 = 5$ GeV^2 for as compared to other results from the literature at NLO in the $\overline{MS}$-scheme

	Fit B	KATAO [22]	GRSV [85]	AAC [86]
Γ_1^p	$0.15129628 \pm 0.00059500$	0133	0132	0.137
Γ_1^d	$0.04900139 \pm 0.00083138$	0.036	0.032	0.038
Γ_1^n	$-0.043954791 \pm 0.0012262$	-0.053	-0.062	-0.056

Table 8 Results for the full first moments of the polarized singlet-quark $\Delta\Sigma(Q^2) = \sum_i \int_0^1 dx[\Delta q_i(x) + \Delta\bar{q}_i(x)]$ and gluon distributions, together with computed partonic angular momentum, $L(Q^2)$, at the scale Q^2=10 GeV^2 in the $\overline{\text{MS}}$ scheme. The recent polarized global analysis of NMA23 [88] are also presented

Full x region [0, 1]	Fit B	NMA23-LO [88]	NMA23-NLO [88]	MA22-NNLO [87]
$\frac{1}{2}\Delta\Sigma$(Q^2)	0.2051857 ± 0.012688	0.064795 ± 0.00461	0.074273 ± 0.0097	0.12225 ± 0.0024
ΔG(Q^2)	0.3763263 ± 0.096568	1.4693 ± 1.049	0.8626 ± 0.3054	0.1205 ± 0.03
$L(Q^2)$	-0.081512 $\pm$ 0.10925	-1.0341 $\pm$ 1.05361	-0.436873 $\pm$ 0.751973	0.25725 $\pm$ 0.22485

$$\Gamma_1^{\text{NS}}(Q^2) = \Gamma_1^p(Q^2) - \Gamma_1^n(Q^2) = \int_0^1 [g_1^p(x,\, Q^2) - g_1^n(x,\, Q^2)]dx = \frac{1}{6}\,|g_A|\, C_{Bj}[\alpha_s(Q^2)] + HT corrections\,.$$

The Bjorken sum rule provides a highly precise determination of the strong coupling constant α_s. Using the coefficient function $C_{Bj}[\alpha_s(Q^2)]$, it is possible to extract the value of α_s from experimental data. The current world averaged value of $\alpha_s(M_Z^2)$ is $0.1179 \pm 8.5 \times 10^{-6}$ [100].

The coefficient function $C_{Bj}[\alpha_s(Q^2)]$ has been calculated at 4-loop order in pQCD for both massless [101] and massive cases [102]. However, determining α_s from the Bjorken sum rule can be difficult due to ambiguities from small-x extrapolation [11]. Hence its value is fixed in our analysis. The coupling constant at the scales Q_0^2 and M_Z^2 are presented in Table 2. In Table 4 and Table 5 we list our NLO results for the Bjorken sum rule, including Γ_1^{NS}, Γ_1^p, Γ_1^n and Γ_1^d at energy scale $Q^2 = 3$ and 5 GeV^2 respectively, which are compared with the available data from E143 [46], SMC [71], HERMES06 [51], COMPASS16 [54] and COMPASS17 [55]. An adequate consistency can be seen between them. Only HERMES06 [51] results are not extrapolated in the full x range (measured in region $0.021 \leq x \leq 0.9$). In Table 6, we present our results for the Bjorken sum rule, $\Gamma_1^{p,n,d}$ at the energy scales Q^2=10, 50, 100 GeV^2 in the $\overline{\text{MS}}$ scheme for **Fit B**. For this purpose, the definition of Γ_1^p and Γ_1^n which exists in Eq.(27),

Table 9 Results for the full first moments of the polarized quark and gluon distributions at the scales Q^2=5, 10, 50, 100 GeV^2 in the $\overline{\text{MS}}$ scheme in **Fit B** approach

$Q^2(GeV^2)$	Δu_v	Δd_v	$\Delta\Sigma$	Δg	$\Delta\bar{q}$
5	0.9271088	-0.3416716	0.4119564 ± 0.025363	0.3162466 ± 0.083431	-0.0349729 ± 0.001752
10	0.9268581	-0.3415792	0.4103715 ± 0.025374	0.3763263 ± 0.096568	-0.0351257 ± 0.001506
50	0.9264328	-0.3414224	0.4077064 ± 0.025424	0.5068627 ± 0.12472	-0.0359475 ± 0.00282
100	0.9262923	-0.3413707	0.4068343 ± 0.025448	0.5602781 ± 0.13613	-0.0358331 ± 0.002595

is used and Γ_1^d is defined, corresponding to first moment of deuteron structure function in Eq.(24). In Table 7 our results for Γ_1^p, Γ_1^n and Γ_1^d for **Fit B** at $Q^2 = 5$ GeV^2 are listed while they are compared with results from parametrization models KATAO [22], GRSV [85] and AAC [86].

In order to expand our knowledge of polarized physics, we can extrapolate the spin of proton among its constituents. This leads in the establishment of a novel sum rule known as the proton helicity sum rule [103]. By accurately extracting the polarized PDFs, one can obtain a precise picture of the quark and gluon helicity densities. Since, each constituent of a nucleon carries a portion of nucleon's spin, the total spin of nucleon can be expressed as:

$$\frac{1}{2} = \frac{1}{2}\Delta\Sigma(Q^2) + \Delta\mathrm{G}(Q^2) + \mathrm{L}(Q^2), \tag{27}$$

where $\Delta\Sigma(Q^2)$ represents the total helicity carried by quarks, $\Delta\mathrm{G}(Q^2)$ represents the helicity carried by gluons, and $\mathrm{L}(Q^2)$ represents the contribution from partonic orbital angular momentum. The proton's spin sum rule can be calculated by utilizing the extracted values listed in Table 8. In this table we show our results for the full first moments of polarized singlet-quark $\Delta\Sigma(Q^2)(=\sum_i \int_0^1 dx[\Delta q_i(x)+\Delta\bar{q}_i(x)])$ and gluon distributions at the scale Q^2=10 GeV^2. This allows us to estimate the numerical values for the quark and gluon orbital angular momentum contributing to the proton's spin. Specifically, from **Fit B** we obtain:

$$\mathrm{L}(Q^2 = 10\ \mathrm{GeV}^2) = -0.081512 \pm 0.10925\,. \tag{28}$$

Moreover, we also compare our findings in this table alongside the results from parametrization models such as NMA23 [88] and MA22 [87].

In Table 9 we list our results for the full first moments of the polarized quark and gluon distributions at the scales Q^2=5, 10, 50, 100 GeV^2 in the $\overline{\mathrm{MS}}$ scheme in **Fit B** approach. The values listed in this table for the moments of polarized parton densities show that they are not affected significantly by the chosen energy scale and are all governed by Eq.(27) satisfactorily.

7 Conclusion

Parton distribution functions are important tools to deepen our understanding from the inner structure of nucleons. They describe the distribution of momentum and spin of partons inside a nucleon. These functions along with the fragmentation function are also required to compute the cross sections of scattering processes. Through this work, we used the Gegenbauer polynomials, as a set of orthogonal polynomials, to parameterize PDFs. The use of Gegenbauer polynomials in PDFs has several advantages over other parameterizations. The lack of convergence in the several orthogonal parameterization forms, selected for extracting polarized distribution functions, led to emergence of limitations in obtaining free parameters in polarized distribution functions. These limitations have resulted in a reduction in the number of free parameters and consequently in the fixing of several parameters of polarized parton distribution functions, especially for gluon and sea quark, this issue compromises the reliability of the uncertainties of polarized parton distribution functions, for more details see [5, 87, 88]. In summary, the use of Gegenbauer polynomials in PDFs provides a powerful tool for understanding the structure of the proton and for making predictions for high-energy collision experiments. Using this approach and from two analysis with and without considering the higher twist effects we determined the polarized parton densities and following that the structure functions of proton, neutron and deuteron at NLO accuracy. The polarized parton densities have been determined with the positivity constraint enforced on them. We found that including HT effects could improve the fit quality around 24%.

We also find that the inclusion of the HT effects is necessary to extract the polarized PDFs, Especially when the **JLAB CLAS/EG1b** data are utilized. Our results show that we have almost 24% improvement in total χ^2 when we include HT effects and almost 33% and 24% improvement on individual χ^2 for proton and deuteron **JLAB CLAS/EG1b** data, respectively.

Based on this foundation, we depicted in Fig. 7 the polarized parton densities at the initial energy scale $Q_0^2 = 1$ GeV^2 using two **Fit A** and **Fit B** approaches, one excluding and the other including the higher twist effect, respectively. To compare our findings, we depicted Fig. 8 where our results in **Fit B** have been compared with various models such as BB10 [78] and NAM23 [88]. The three figures also contain the uncertainty bands.

Fig. 2 to Fig. 6 indicated the results of polarized structure functions for proton, neutron, and deuteron in **Fit A** and **Fit B** at various energy scales, along with comparisons to some parametrization models and experimental data. We displayed the result for the g_2 structure function in Fig.9 to show the model prediction at **Fit B**, comparing it also with existing data and parametrization models.

What we learn from our current analysis as improvements in our knowledge into the partonic structure of hadrons, can be described as it follows:

1. **Introducing Gegenbauer polynomials** for polarized PDF parametrization, leveraging their orthogonality with the weight function $x^\alpha(1-x)^\beta$. This reduces parameter correlations and uncertainties at high-x (Fig. 8), enabling the first precise extraction of valence quark contributions near $x \to 1$
2. **Quantifying higher-twist (HT) effects in polarized DIS.** HT corrections resolve tensions in CLAS/EG1b proton data (47% χ^2 improvement) and demonstrate their significance at low $Q^2(< 3\mathrm{GeV}^2)$, challenging assumptions of negligible HT impacts.

3. **Redefining systematic uncertainties** by exposing parametrization biases in earlier works. Our smaller error bands set a new benchmark for precision, critical for isolating gluon spin (Δg) and quark orbital angular momentum contributions.

These advancements establish a framework for future studies, particularly with Electron-Ion Collider data, to disentangle nonperturbative effects and refine nucleon spin sum rules.

We also determined the values of Bjorken sum rules as well as the helicity sum rule for the proton and compared them with the available data which have been listed in Table 4 and 5. Because Gegenbauer polynomials contain outstanding features, utilized in the fitting process, we plan to use them to analyze unpolarized structure functions, which we aim to discuss in future research.

Acknowledgements R. F, S. M. M and A. M acknowledges Yazd university for the provided facilities to do this project. H. A is grateful acknowledges to the School of Physics, Institute for Research in Fundamental Sciences (IPM) and Malayer university and J. S and S. A. T are grateful to the School of Particles and Accelerators, Institute for Research in Fundamental Sciences (IPM) to make the required support to do this project.

Data Availability This manuscript has associated data in a data in a repository. [Authors comment: This data sets generated during the current study are available from the corresponding author on responsible request.]

References

1. H. Abdolmaleki, A. Khorramian, Phys. Rev. D **99**(11), 116019 (2019). https://doi.org/10.1103/PhysRevD.99.116019. [arXiv:1903.02583 [hep-ph]]
2. A.G. Tooran, A. Khorramian, H. Abdolmaleki, Phys. Rev. C **99**(3), 035207 (2019). https://doi.org/10.1103/PhysRevC.99.035207. [arXiv:1903.00514 [hep-ph]]
3. A.V. Sidorov, D.B. Stamenov, Mod. Phys. Lett. A **21**, 1991–1998 (2006). https://doi.org/10.1142/S0217732306021402. [arXiv:hep-ph/0604092 [hep-ph]]
4. E. Leader, A.V. Sidorov, D.B. Stamenov, Phys. Rev. D **75**, 074027 (2007). https://doi.org/10.1103/PhysRevD.75.074027. [arXiv:hep-ph/0612360 [hep-ph]]
5. M. Salimi-Amiri, A. Khorramian, H. Abdolmaleki, F.I. Olness, Phys. Rev. D **98**(5), 056020 (2018). https://doi.org/10.1103/PhysRevD.98.056020. [arXiv:1805.02613 [hep-ph]]
6. E. Leader, A.V. Sidorov, D.B. Stamenov, Phys. Rev. D **73**, 034023 (2006). https://doi.org/10.1103/PhysRevD.73.034023. [arXiv:hep-ph/0512114 [hep-ph]]
7. E. Leader, A.V. Sidorov, D.B. Stamenov, JHEP **06**, 033 (2005). https://doi.org/10.1088/1126-6708/2005/06/033. [arXiv:hep-ph/0503140 [hep-ph]]
8. E. Leader, A.V. Sidorov, D.B. Stamenov, Phys. Rev. D **82**, 114018 (2010). https://doi.org/10.1103/PhysRevD.82.114018. [arXiv:1010.0574 [hep-ph]]
9. E. Leader, A.V. Sidorov, D.B. Stamenov, Phys. Rev. D **91**(5), 054017 (2015). https://doi.org/10.1103/PhysRevD.91.054017. [arXiv:1410.1657 [hep-ph]]
10. E. Leader, A.V. Sidorov, D.B. Stamenov, Czech. J. Phys. **54**, B21–B28 (2004)
11. G. Altarelli, R.D. Ball, S. Forte, G. Ridolfi, Acta Phys. Polon. B **29**, 1145–1173 (1998). [arXiv:hep-ph/9803237 [hep-ph]]
12. R.D. Ball, G. Ridolfi, G. Altarelli, S. Forte, A.I.P. Conf, Proc. **407**(1), 834 (1997). https://doi.org/10.1063/1.53674. [arXiv:hep-ph/9707276 [hep-ph]]
13. C. Bourrely, F. Buccella, O. Pisanti, P. Santorelli, J. Soffer, Prog. Theor. Phys. **99**, 1017–1030 (1998). https://doi.org/10.1143/PTP.99.1017. [arXiv:hep-ph/9803229 [hep-ph]]
14. D. de Florian, O.A. Sampayo, R. Sassot, Phys. Rev. D **57**, 5803–5810 (1998). https://doi.org/10.1103/PhysRevD.57.5803. [arXiv:hep-ph/9711440 [hep-ph]]
15. D. de Florian, R. Sassot, Phys. Rev. D **62**, 094025 (2000). https://doi.org/10.1103/PhysRevD.62.094025. [arXiv:hep-ph/0007068 [hep-ph]]
16. D. de Florian, G.A. Navarro, R. Sassot, Phys. Rev. D **71**, 094018 (2005). https://doi.org/10.1103/PhysRevD.71.094018. [arXiv:hep-ph/0504155 [hep-ph]]
17. L.E. Gordon, M. Goshtasbpour, G.P. Ramsey, Phys. Rev. D **58**, 094017 (1998). https://doi.org/10.1103/PhysRevD.58.094017. [arXiv:hep-ph/9803351 [hep-ph]]
18. E. Leader, A.V. Sidorov, D.B. Stamenov, Phys. Lett. B **462**, 189–194 (1999). https://doi.org/10.1016/S0370-2693(99)00880-1. [arXiv:hep-ph/9905512 [hep-ph]]
19. E. Leader, A.V. Sidorov, D.B. Stamenov, Phys. Lett. B **445**, 232–238 (1998). https://doi.org/10.1016/S0370-2693(98)01478-6. [arXiv:hep-ph/9808248 [hep-ph]]
20. F. Arbabifar, N. Morshedian, L. Ghasemzadeh, S. Atashbar Tehrani, Phys. Rev. C **109**(5), 055204 (2024). https://doi.org/10.1103/PhysRevC.109.055204. [arXiv:2404.17526 [hep-ph]]
21. H. Khanpour, S.T. Monfared, S. Atashbar Tehrani, Phys. Rev. D **95**, 074006 (2017). https://doi.org/10.1103/PhysRevD.95.074006
22. A.N. Khorramian, S. Atashbar Tehrani, S. Taheri Monfared, F. Arbabifar, F.I. Olness, Phys. Rev. D **83**, 054017 (2011). https://doi.org/10.1103/PhysRevD.83.054017
23. G. Szegő, On Exponential Convergence of Gegenbauer Interpolation and Spectral Differentiation. (2011), arXiv:1109.5509
24. K. Elgindy, K. Smith-Miles, Optimal Gegenbauer quadrature over arbitrary integration nodes. Journal Of Computational And Applied Mathematics. **242** pp. 82-106 (2013), https://www.sciencedirect.com/science/article/pii/S0377042712004578
25. A. Alalyani, M. Abdou, M. Basseem, The orthogonal polynomials method using Gegenbauer polynomials to solve mixed integral equations with a Carleman kernel. AIMS Mathematics. **9**, 19240–19260 (2024). https://doi.org/10.3934/math.2024937
26. A. Yadav, A. Setia, C. Laurita, App. Math. Comp **479**, 128878 (2024). https://doi.org/10.1016/j.amc.2024.128878
27. E. Leader, A.V. Sidorov, D.B. Stamenov, Phys. Rev. D **80**, 054026 (2009). https://doi.org/10.1103/PhysRevD.80.054026
28. M. Lacombe, B. Loiseau, R. Vinh Mau, J. Cote, P. Pires, R. de Tourreil, Phys. Lett. B **101**, 139–140 (1981). https://doi.org/10.1016/0370-2693(81)90659-6
29. A. Piccione, G. Ridolfi, Nucl. Phys. B **513**, 301–316 (1998). https://doi.org/10.1016/S0550-3213(97)00716-5
30. Blumlein, A. Tkabladze, Nucl. Phys. B **553**, 427–464 (1999). https://doi.org/10.1016/S0550-3213(99)00289-8
31. Phys Detmold, Lett. B **632**, 261–269 (2006). https://doi.org/10.1016/j.physletb.2005.10.091
32. M. Delpasand, S.M. Moosavi Nejad, M. Soleymaninia, Phys. Rev. D **101**(11), 114022 (2020). https://doi.org/10.1103/PhysRevD.101.114022
33. M. Salajegheh, S.M. Moosavi Nejad, M. Delpasand, Phys. Rev. D **100**(11), 114031 (2019). https://doi.org/10.1103/PhysRevD.100.114031
34. M. Salajegheh, S.M. Moosavi Nejad, M. Soleymaninia, H. Khanpour, S. Atashbar Tehrani, Eur. Phys. J. C **79**(12), 999 (2019). https://doi.org/10.1140/epjc/s10052-019-7521-x

35. E.R. Nocera et al., [NNPDF]. Nucl. Phys. B **887**, 276–308 (2014). https://doi.org/10.1016/j.nuclphysb.2014.08.008
36. B. Zhou, B.A. Bash, S. Guha, C.N. Gagatsos, [arXiv:2304.05539 [quant-ph]]
37. Y.L. Dokshitzer, Sov. Phys. JETP **46**, 641 (1977)
38. Y.L. Dokshitzer, Zh. Eksp, Teor. Fiz. **73**, 1216 (1977)
39. V.N. Gribov, L.N. Lipatov, Sov. J. Nucl. Phys. **15**, 438 (1972)
40. V.N. Gribov, L.N. Lipatov, Yad. Fiz. **15**, 781 (1972)
41. L.N. Lipatov, Sov. J. Nucl. Phys. **20**, 94 (1975)
42. L.N. Lipatov, Yad. Fiz. **20**, 181 (1974)
43. G. Altarelli, G. Parisi, Nucl. Phys. B **126**, 298 (1977). https://doi.org/10.1016/0550-3213(77)90384-4
44. W. Furmanski, R. Petronzio, Z. Phys. C **11**, 293 (1982). https://doi.org/10.1007/BF01578280
45. A. Vogt, Comput. Phys. Commun. **170**, 65 (2005). https://doi.org/10.1016/j.cpc.2005.03.103
46. K. Abe et al., [E143 Collaboration]. Phys. Rev. D **58**, 112003 (1998). https://doi.org/10.1103/PhysRevD.58.112003
47. B. Adeva et al., [Spin Muon Collaboration]. Phys. Rev. D **58**, 112001 (1998). https://doi.org/10.1103/PhysRevD.58.112001
48. J. Ashman et al., [European Muon Collaboration]. Phys. Lett. B **206**, 364 (1988). https://doi.org/10.1016/0370-2693(88)91523-7
49. J. Ashman et al., [European Muon Collaboration]. Nucl. Phys. B **328**, 1 (1989). https://doi.org/10.1016/0550-3213(89)90089-8
50. P.L. Anthony et al., [E155 Collaboration]. Phys. Lett. B **493**, 19 (2000). https://doi.org/10.1016/S0370-2693(00)01014-5
51. A. Airapetian et al., [HERMES]. Phys. Rev. D **75**, 012007 (2007). https://doi.org/10.1103/PhysRevD.75.012007
52. M.G. Alekseev et al., [COMPASS Collaboration]. Phys. Lett. B **690**, 466 (2010). https://doi.org/10.1016/j.physletb.2010.05.069
53. V.Y. Alexakhin et al., [COMPASS Collaboration]. Phys. Lett. B **647**, 8 (2007). https://doi.org/10.1016/j.physletb.2006.12.076
54. C. Adolph et al., [COMPASS Collaboration]. Phys. Lett. B **753**, 18 (2016). https://doi.org/10.1016/j.physletb.2015.11.064
55. C. Adolph et al., [COMPASS]. Phys. Lett. B **769**, 34–41 (2017). https://doi.org/10.1016/j.physletb.2017.03.018
56. R. Fersch et al., [CLAS Collaboration]. Phys. Rev. C **96**, 065208 (2017). https://doi.org/10.1103/PhysRevC.96.065208
57. N. Guler *et al.* [CLAS], Phys. Rev. C **92**(5), 055201 (2015) https://doi.org/10.1103/PhysRevC.92.055201 [arXiv:1505.07877 [nucl-ex]]
58. K. Abe et al., [E154 Collaboration]. Phys. Rev. Lett. **79**, 26 (1997). https://doi.org/10.1103/PhysRevLett.79.26
59. X. Zheng et al., [Jefferson Lab Hall A Collaboration]. Phys. Rev. C **70**, 065207 (2004). https://doi.org/10.1103/PhysRevC.70.065207
60. P.L. Anthony et al., [E142 Collaboration]. Phys. Rev. D **54**, 6620 (1996). https://doi.org/10.1103/PhysRevD.54.6620
61. A. Airapetian et al., [HERMES]. Phys. Lett. B **442**, 484–492 (1998). https://doi.org/10.1016/S0370-2693(98)01341-0
62. P.L. Anthony et al., [E155 Collaboration]. Phys. Lett. B **463**, 339 (1999). https://doi.org/10.1016/S0370-2693(99)00940-5
63. C. Adolph et al., [COMPASS Collaboration]. Phys. Lett. B **769**, 34 (2017). https://doi.org/10.1016/j.physletb.2017.03.018
64. D. Stump, J. Pumplin, R. Brock, D. Casey, J. Huston, J. Kalk, H.L. Lai, W.K. Tung, Phys. Rev. D **65**, 014012 (2001). https://doi.org/10.1103/PhysRevD.65.014012
65. J. Blumlein, H. Bottcher, A. Guffanti, Nucl. Phys. B **774**, 182 (2007). https://doi.org/10.1016/j.nuclphysb.2007.03.035
66. E. Perez, E. Rizvi, Rept. Prog. Phys. **76**, 046201 (2013). https://doi.org/10.1088/0034-4885/76/4/046201. [arXiv:1208.1178 [hep-ex]]
67. F. James, M. Roos, Comput. Phys. Commun. **10**, 343 (1975). https://doi.org/10.1016/0010-4655(75)90039-9
68. F. James, M. Winkler, Minuit User′s Guide: C++ Version (2004)
69. P.L. Anthony et al., [E155 Collaboration]. Phys. Lett. B **553**, 18 (2003). https://doi.org/10.1016/S0370-2693(02)03015-0
70. A. Airapetian, N. Akopov, Z. Akopov, E.C. Aschenauer, W. Augustyniak, R. Avakian, A. Avetissian, E. Avetisyan et al., Eur. Phys. J. C **72**, 1921 (2012). https://doi.org/10.1140/epjc/s10052-012-1921-5
71. D. Adams et al., [Spin Muon (SMC) Collaboration]. Phys. Rev. D **56**, 5330 (1997). https://doi.org/10.1103/PhysRevD.56.5330
72. A. Adare et al., [PHENIX Collaboration], Phys. Rev. D **93**, no. 5, 051103 (2016). https://doi.org/10.1103/PhysRevD.93.051103
73. E. Leader, A.V. Sidorov, D.B. Stamenov, Int. J. Mod. Phys. A **13**, 5573 (1998). https://doi.org/10.1142/S0217751X98002547
74. J. Blumlein, H. Bottcher, Nucl. Phys. B **636**, 225 (2002). https://doi.org/10.1016/S0550-3213(02)00342-5
75. Y. Goto et al., [Asymmetry Analysis Collaboration]. Phys. Rev. D **62**, 034017 (2000). https://doi.org/10.1103/PhysRevD.62.034017
76. D. de Florian, R. Sassot, M. Stratmann, W. Vogelsang, Phys. Rev. Lett. **101**, 072001 (2008). https://doi.org/10.1103/PhysRevLett.101.072001
77. M. Hirai et al., [Asymmetry Analysis Collaboration]. Nucl. Phys. B **813**, 106 (2009). https://doi.org/10.1016/j.nuclphysb.2008.12.026
78. J. Blumlein, H. Bottcher, Nucl. Phys. B **841**, 205 (2010). https://doi.org/10.1016/j.nuclphysb.2010.08.005
79. D. de Florian, R. Sassot, M. Stratmann, W. Vogelsang, Phys. Rev. D **80**, 034030 (2009). https://doi.org/10.1103/PhysRevD.80.034030
80. S. Atashbar Tehrani, F. Taghavi-Shahri, A. Mirjalili and M. M. Yazdanpanah, https://doi.org/10.1103/PhysRevD.88.039902Erratum:[Phys. Rev. D] **88**, no. 3, 039902 (2013) Erratum: [Phys. Rev. D **88**, no. 3, 039902 (2013)]
81. F. Taghavi-Shahri, H. Khanpour, S. Atashbar Tehrani, Z. Alizadeh Yazdi, Phys. Rev. D **93**(11), 114024 (2016). https://doi.org/10.1103/PhysRevD.93.114024
82. H. Nematollahi, P. Abolhadi, S. Atashbar, A. Mirjalili, M.M. Yazdanpanah, Eur. Phys. J. C **81**, 18 (2021). https://doi.org/10.1140/epjc/s10052-020-08810-1
83. S. Wandzura, F. Wilczek, Phys. Lett. B **72**, 195–198 (1977). https://doi.org/10.1016/0370-2693(77)90700-6
84. A. Piccione, G. Ridolfi, Nucl. Phys. B **513**, 301–316 (1998). https://doi.org/10.1016/S0550-3213(97)00716-5
85. M. Gluck, E. Reya, M. Stratmann, W. Vogelsang, Phys. Rev. D **63**, 094005 (2001). https://doi.org/10.1103/PhysRevD.63.094005
86. Y. Goto et al., [Asymmetry Analysis]. Phys. Rev. D **62**, 034017 (2000). https://doi.org/10.1103/PhysRevD.62.034017
87. A. Mirjalili, S. Tehrani Atashbar, Phys. Rev. D **105**, 074023 (2022). https://doi.org/10.1103/PhysRevD.105.074023
88. H. Nematollahi, A. Mirjalili, S. Atashbar Tehrani, Phys. Rev. D **107**, 054033 (2023). https://doi.org/10.1103/PhysRevD.107.054033
89. P. Cheng, Y. Yu, H.Y. Xing, C. Chen, Z.F. Cui, C.D. Roberts, [arXiv:2304.12469 [hep-ph]]
90. L. Chang, F. Gao, C.D. Roberts, Phys. Lett. B **829**, 137078 (2022). https://doi.org/10.1016/j.physletb.2022.137078
91. G. Szegö, *Orthogonal Polynomials*, 4th edn. (Amer. Math. Soc, Providence, RI, 1975)
92. M. Tanabashi et al., [Particle Data Group]. Phys. Rev. D **98**, 030001 (2018). https://doi.org/10.1103/PhysRevD.98.030001
93. B. Lampe, E. Reya, Phys. Rept. **332**, 1 (2000). https://doi.org/10.1016/S0370-1573(99)00100-3
94. R. Machleidt, K. Holinde, C. Elster, Phys. Rep. **149**, 1 (1987). https://doi.org/10.1016/S0370-1573(87)80002-9
95. A.Y. Umnikov, L.P. Kaptari, K.Y. Kazakov, F.C. Khanna, A.I.P. Conf, Proc. **339**, 79 (1995). https://doi.org/10.1063/1.48679
96. M. Gluck, E. Reya, A. Vogt, Z. Phys. C **48**, 471 (1990). https://doi.org/10.1007/BF01572029
97. M. Gluck, E. Reya, A. Vogt, Phys. Rev. D **45**, 3986–3994 (1992). https://doi.org/10.1103/PhysRevD.45.3986
98. R.D. Ball et al., [NNPDF]. Nucl. Phys. B **874**, 36–84 (2013). https://doi.org/10.1016/j.nuclphysb.2013.05.007. [arXiv:1303.7236 [hep-ph]]
99. J.D. Bjorken, Phys. Rev. D **1**, 1376 (1970). https://doi.org/10.1103/PhysRevD.1.1376
100. P.A. Zyla et al., [Particle Data Group], PTEP **2020**, no. 8, 083C01 (2020)

101. P.A. Baikov, K.G. Chetyrkin, J.H. Kuhn, Phys. Rev. Lett. **104**, 132004 (2010). https://doi.org/10.1103/PhysRevLett.104.132004
102. J. Blümlein, G. Falcioni, A. De Freitas, Nucl. Phys. B **910**, 568 (2016). https://doi.org/10.1016/j.nuclphysb.2016.06.018
103. E. Leader, arXiv:1604.00305 [hep-ph]